SYNCHROTRON RADIATION/LASERS AND DOUBLY-EXCITED ATOMS

W-J CHEN, T. K. FANG, Y. K. HO, C. K. NI AND A. H. KUNG
Institute of Atomic and Molecular Sciences, Academia Sinica, Taipei
TAIWAN, ROC 17064
E-mail: Akung@po.iams.sinica.edu.tw

T. S. YIH, H. S. FUNG, C. C. CHU AND H. H. WU
Department of Physics, National Central University, Chung-Li, TAIWAN
ROC 32054
E-mail: tsyih@joule.phy.ncu.edu.tw

T. N. CHANG
Department of Physics and Astronomy, University of Southern California
Los Angeles, CA 90089-0484, USA
E-mail: tnchang@usc.edu

1 Introduction

This report highlights a series of joint theoretical and experimental collaborations which started over ten years ago in Taiwan. The recent topic program *Synchrotron Radiation and Multiply-excited Atoms*, sponsored by the National Center for Theoretical Sciences (NCTS) at Tsinghua University in Hsinchu and organized by K. T. Chung and C. S. Hsu, offers an excellent opportunity for many of us to work together at times from July to December of 1998 on some of the projects that have been of interests to us during the past decade. The experimental efforts presented in this report involve the VUV projects carried out at the Synchrotron Radiation Research Center (SRRC) in Hsinchu by Tai-sone Yih and his research group at the National Central University (NCU) in Chungli and the untra-high resolution laser measurements led by Andy Kung at the Institute of Atomic and Molecular Sciences (IAMS), Academia Sinica. The theoretical efforts include works using the B-spline-based configuration interaction (BSCI) and multichannel K-matirx (BSK) approaches by Tu-nan Chang and his theory group at the University of Southern California and the complex-rotation method by Yew Kam Eugene Ho at IAMS. Many of the theoretical results presented in this report are the works of Te-Kuei Fang at IAMS in collaboration with Chang and Ho. We will limit our discussion in this report to the atomic processes dominated by the *doubly-excited* states. The atomic process involving triply excited states will be reported in a companion paper *Multiply Excited States in Lithium* in this volume by J. C. Chang and K. T. Chung.

In 1986, Chang and his co-workers started a series of theoretical calculations on atomic transitions involving two-electron and divalent (e.g., alkaline-earth) atoms

[1, 2] in an attempt to understand in detail the atomic processes which manifest the strong multi-electron interactions. For example, at an energy immediately above the first ionization threshold, the spectra of an alkaline-earth atom are dominated by the strongly energy-dependent doubly-excited autoionization states. The photoabsorption/photoionization spectra of these divalent systems are characterized typically by two types of asymmetric autoionization series, one broad and one narrow in width, caused by the simultaneous change of electronic orbitals of two outer electrons in a double-excitation process [3, 4].

Shortly after the initial work by Chang and Kim [1], Yih initiated an experimental VUV photoabsorption program to measure the *absolute* cross section of metal vapors at NCU. Unlike the permanent gas which stays in gas phase at room temperature, metal vapors are far more reactive and need to be heated to a fairly high temperature for a sufficient vapor density in a photoabsorption experiment. A reliable *absolute* cross section measurement for metal vapor relies critically on an accurate determination of the column density along the interaction path. A conventional laboratory VUV light source was first employed in Yih's earlier experiments [5]. The use of more intense synchrotron radiation light source at SRRC and the steadily improved instrumentation under a more controlled environment by Yih and his co-workers have successfully reduced the experimental uncertainty over a factor of two during the past decade [6]. The continuous interplay between theory and experiment has provided the necessary impetus for more activities and further refinements.

Whereas the VUV light source from the synchrotron radiation, with its extended spectral region, works extremely well in the study of resonance structure which has a width as small as a few meV, it does not have the necessary energy resolution to observe some of the *ultra-narrow* resonances predicated by the theoretical calculation. One of such examples is the ultra-narrow doubly excited $3p\nu g\ ^1F$ autoionization series which interferes strongly with an overlapping broad $3p\nu d\ ^1F$ series, proposed by Fang *et al* [7], in the calculated photoionization spectra of Mg-like Al^+ from the bound excited $3s\nu_i d\ ^1D$ states. At a post seminar discussion following a talk presented by Chang a few years ago at IAMS, Kung proposed that a multistep multicolor lasers experiment, with an energy resolution about two to three orders of magnitude better than the best in synchrotron radiation, be set up at IAMS to investigate such ultra-narrow $3p\nu g\ ^1F$ resonances in Mg. A joint experimental effort between Kung's group at IAMS and Yih's group at NCU proves to be a great success when these resonances were clearly observed last year for the first time [8]. In Sec. 2, the most recent progress on the study of these ultra-narrow doubly-excited $3p\nu g\ ^1F$ resonances is presented.

On the theory side, the BSCI approach for a single continuum [2, 9] has been extended successfully by Fang and Chang to multiple continua with a B-spline-based multichannel K-matrix approach (BSK) [10]. Its application to Mg doubly-excited spectra above the second ionization threshold has led to a more definitive physical interpretation for a few very interesting resonance features which were observed recently by Yih's group [11]. In Sec. 3, we present a summary of what we have learned from this joint experimental and theoretical project.

In addition to the theoretical development of the BSK approach, the BSCI approach has also been incorporated recently into the well established complex-rotation method by Fang and Ho at IAMS. Of particular interest is its application to the photoionization of two-electron atom in the presence of an external dc electric field [12]. The result of a study on the field effect to photoionization by Fang and Ho is presented in Sec. 4. It is hoped that, similar to the earlier theoretical BSCI calculations, the theoretical work on photoionization in external field may stimulate the experimental work in the near future.

2 Ultra-narrow Doubly-excited Resonances in Alkaline-earth Atoms

For many years, Chang and his co-workers have performed extensive BSCI calculations to quantify the photoionization of Mg and Mg-like ions from their bound excited states. These calculations are a part of a concerted effort to provide precise physical interpretation of multielectron interaction in many-electron systems. One of the most interesting physical features suggested by these studies is the interference between the overlapping $3p\nu d\ ^1F$ and the $3p\nu g\ ^1F$ autoionization series [7, 13]. Calculations show that the strong $3s\nu_i d\ ^1D$ to $3p\nu d\ ^1F$ transition is dominated by the *shakeup* of the outer $\nu_i d$ electron following a bound-bound $3s$ to $3p$ excitation. The calculations also show the presence of extremely narrow $3p\nu g\ ^1F$ resonances located on top of the broad $3p\nu d\ ^1F$ resonances. The characteristics of the $3s\nu_i d\ ^1D$ to $3p\nu g\ ^1F$ resonances result primarily from the energy variation of the bound component of the final state wave function in the vicinity of the $3p\nu g\ ^1F$ resonance and are not dominated by contribution of the transition from the initial bound state to the continuum component of the final state wave function.

In this section, we report the progress of a multistep multicolor laser study of doubly-excited resonances in alkaline-earth atoms, aimed at providing a quantitative comparison of experiments and theoretical calculations as exemplified by the $3s\nu_i d\ ^1D$ to the $3p\nu l\ ^1F$ autoionization spectra in Mg.

2.1 Experiment

The experimental approach follows that initially employed by Cooke *et al.* in what they described as an isolated-core excitation scheme [14, 15]. As shown schematically in Fig. 1, population in the $3s\nu_i d\ ^1D$ states is prepared by sequential excitation of an effusive beam of atomic Mg. A single-longitudinal-mode laser tuned to the $3s^2\ ^1S$ to $3s3p\ ^1P$ resonance excites the atom from its ground state to the $3s3p\ ^1P$ state. After a short time delay, pulses from a second laser transfers a portion of this population from the $3s3p\ ^1P$ state to a $3s\nu_i d\ ^1D$ state. A third laser then is used to photoionize the atom from the ^1D state. The laser is scanned to probe for autoionization resonances resulting from the $3s\nu_i d\ ^1D$ to $3p\nu g\ ^1F$ transitions. A time-of-flight mass spectrometer is used to detect the Mg ions. The laser wavelength is calibrated using the laser's built-in wavemeter and an external CW wavemeter to an accuaracy of 0.01 cm^{-1}. The energies of the intermediate levels of Mg are

obtained from published data and are accurate to 0.01 cm^{-1} [16]. Experiments are performed for $\nu_i = 3$ to 6 and $\nu = 5$ to 7. A total of 5 resonances are observed and their lineshapes and widths are measured.

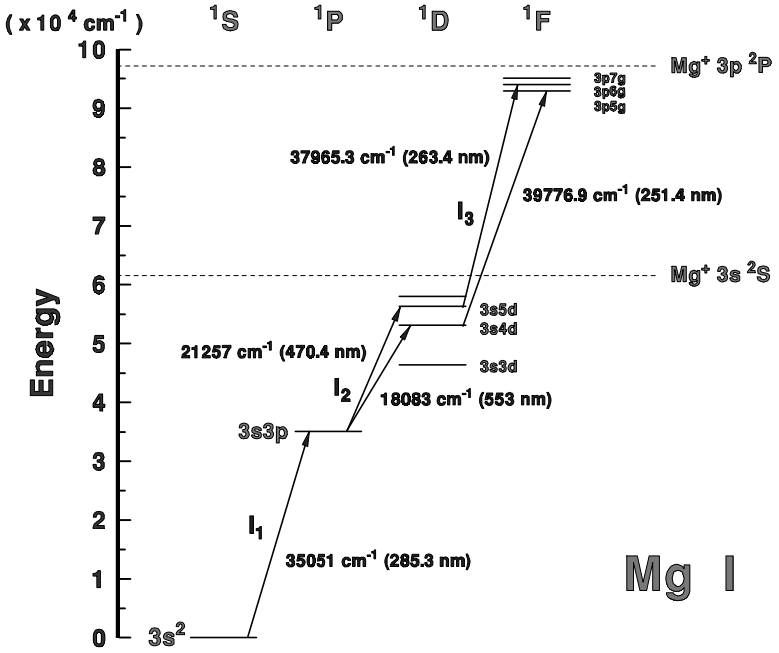

Figure 1. Schematic diagram for the multistep three-color experiment.

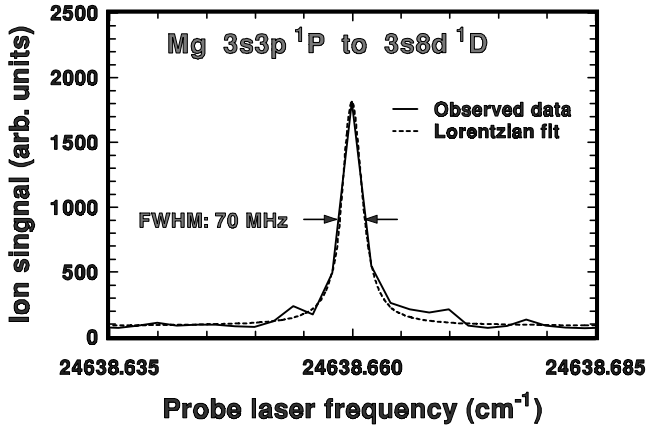

Figure 2. High-resolution resonance-enhanced *1+1* photoionization spectrum of the $3s3p\ ^1P$ state in the vicinity of the $3s8d\ ^1D$ intermediate state.

2.2 Results and Discussion

Preliminary results of the investigation are presented. The first step is to determine the spectral resolution of the entire set-up. Population in the $3s3p\ ^1P$ level is ionized by resonance-enhanced *1+1* ionization via the $3s8d\ ^1D$ state. Fig. 2 shows the ion signal recorded as the probe laser is scanned. The signal is fitted to a Lorentzian profile to give a spectral full-width-half-maximum of 70 MHz [17]. Since the lifetime of the $3s8d\ ^1D$ state is about 50 nsec., which corresponds to a Fourier-transformed frequency width of 3.2 MHz, this width is a measurement of the instrumental resolution. This value can be extrapolated for the laser wavelengths used in the autoionization measurements to give a resolution of 84.5 MHz for those measurements.

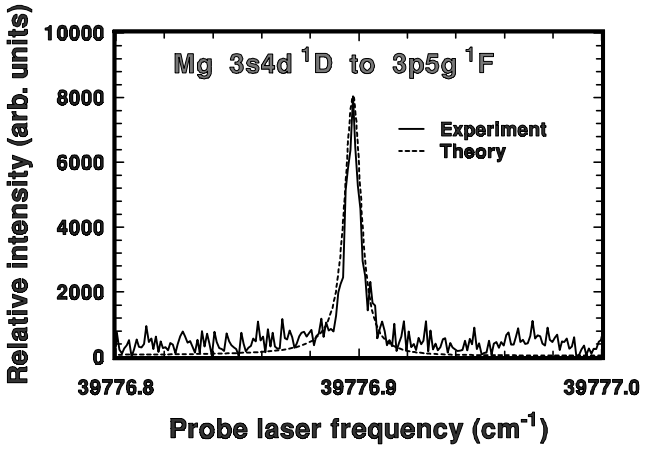

Figure 3. Mg $3s4d\ ^1D$ to $3p5g\ ^1F$ spectrum. The dotted BSCI theoretical result is convoluted with an instrument resolution of 84.5 MHz. The peak height and energy position of the resonance from theory and experiment are matched.

Fig. 3 is a representative spectrum of the autoionization process. The resonance is that of the $3s4d\ ^1D$ to $3p5g\ ^1F$ transition. The position of the peak of the line is determined from the wavelength of the laser and the known position of the lower level of the transition. The width of the transition is determined by fitting the measured lineshape to a Lorentzian lineshape. Assumption of a Lorentzian lineshape is reasonable since the observed spectral lines have a high degree of symmetry in all cases. Also displayed in Fig. 3 is the result of a BSCI calculation of the ionization cross section from the $3s4d\ ^1D$ state in the same region of the spectrum. To obtain a comparison of the lineshapes, the peak cross-section is matched to the position and the height of the peak ion signal. The calculated results have also been convoluted

with the instrument resolution. Altogether five resonances have been observed. The measured transition energies and the transition energies obtained from the BSCI calculations are shown in Table 1. In comparison, the experimental results are generally to the red side of the calculated values. However, the difference between the experimental values and the calculations is small, of the order of 100 cm^{-1} to 150 cm^{-1}, and is only about 0.2% of the total energy of the observed energy level. The measured linewidths of the $5g$ and $6g$ levels are approximately 250 MHz and 350 MHz respectively, and are in agreement with the calculations (212 MHz and 316 MHz, respectively) to within the experimental uncertainty of 50 MHz. For the $7g$ level, the measured value is larger by about 30% than the calculated value. These linewidths indicate a total lifetime of about 0.5 nsec for the $3p\nu g\ ^1F$ levels. This is quite long for a level that is 4 eV above the ionization continuum. The lifetime of the $3p\nu g\ ^1F$ to the $3s\nu g\ ^1G$ radiative transitions are expected to be similar to the $3s3p\ ^1P$ to $3s^2\ ^1S$ decay (i.e., about 1.2 nsec.) Hence fluorescence emission from the $3p\nu g\ ^1F$ levels to the $3s\nu g\ ^1G$ levels is not negligible and the ionization yield from the ^1F will not be close to 100%.

Table 1. The $3s\nu_i d\ ^1D$ to $3p\nu g\ ^1F$ transition energies (in cm^{-1}).

Initial state	Final state					
ν_i	$\nu = 5$		$\nu = 6$		$\nu = 7$	
	measured	theory	measured	theory	measured	theory
3	46508.5	46660.1	47870.7	47983.7	48687.9	48783.4
4	39777.0	39928.5	41139.1	41252.1	41956.3	42051.9
5	36603.2	36754.8	37965.3	38078.4	38782.6	38878.1
6	34888.3	35039.9	36250.5	36363.5	37067.7	37163.3

Instead of matching the peak height of the measured ionization signal to the calculated $3p5g\ ^1F$ resonance peak, in Fig. 4, the ionization signal is plotted with the baseline (or background ionization signal) matched to the calculated cross-section value at 1.5 GHz away from the peak frequency. It becomes apparent that there is a large difference in the relative maximum measured signal and the relative calculated peak ionization cross-section. In the experiment, the observed ion signal is the total ion signal produced by the probe laser beam. The photon energy of the probe laser is sufficient to ionize the Mg atom from any of its excited states. Some states can be populated due to decay of the initial $3s4d\ ^1D$ state. For the present case, the states that are energetically allowed are the $3s3p\ ^1P$ and the $3s4s\ ^1S$ states. Since ionization from these states must be to the continuum, the cross-section is small compared to the process being studied. The estimated contribution of this continuum ionization to the total signal is less than 10%. Another possibility is the existence of a strong nearby resonance. The BSCI calculations have been performed

for all possible cases and it shows that the tail absorption/ionization from nearby resonances is negligible. Hence this anomaly is not resolved at this time and suggests further study is required. Experiments and calculations are planned to try to resolve this discrepancy.

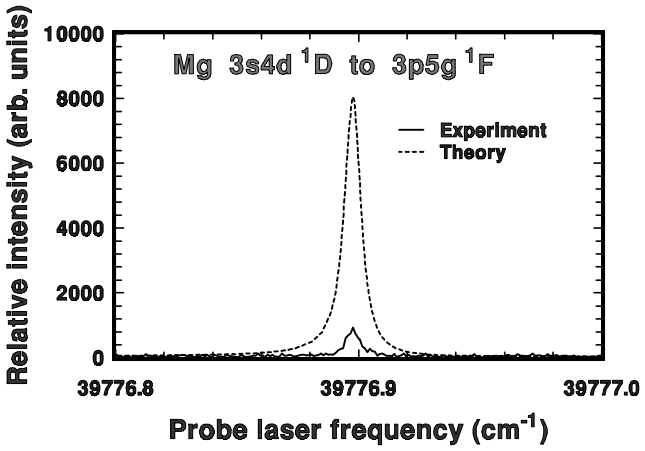

Figure 4. Same spectrum shown in Fig. 3 except that the experiment ion signals are matched with the theorey at the baseline.

In summary, it is significant that the dominant evidence from the present study is that experiment and theory agree to a large extent. It supports the physical interpretation suggested by the BSCI theory leading to the autoionization of the doubly-excited $3p\nu d\ ^1F$ and $3p\nu g\ ^1F$ resonances. The multistep multicolor laser experiment, with its ultrahigh energy resolution, offers a powerful alternative in the VUU region to study the *ultra-narrow* resonances which are unresolved even with the most advanced synchrotron radiation light source.

3 Absolute Photoabsorption Cross Sections from Mg Ground State

In this section, we present the results of a joint experimental and theoretical study on the *absolute* photoabsorption cross sections from the ground state of Mg. We will focus our discussion on a few selected features associated with the doubly-excited resonances with a resonance width substantially broader than the narrow resonances discussed in previsous section. The physical interpretations of spectral profiles presented in this section, supported by a close agreement between theory and experiment, are derived from a detailed theoretical analysis based on the BSK calculation outlined elsewhere [10, 11].

3.1 Experiment

The synchrotron radiation source at SRRC in Hsinchu, Taiwan is employed as the continuum background. The instrumental set-up is similar to the one described in [6]. Depending upon the spectral region, the transmitted light was detected either by a channeltron or a solar blind photomultiplier tube. The spectral bandwidth of the monochromator was set to 0.08 nm in a typical experimental run. The temperature profile along the heatpipe furnance is monitored using 25 pairs of k-type thermocouples. This temperature profile is used later to determine more precisely the column density in the heatpipe. A windowless heatpipe furnace is used in a spectral region with wavelengths shorter than 110 nm. For the present measurement, the LiF windows shown in Fig. 1 of Ref. [6] are replaced by differential pumping systems which keep the heatpipe gas-locked and the monochromator along the synchrotron beam line under an optimal vacuum. Vacuum gauge data read from several positions along the system prove that it works as if it has a buffer gas window.

For the Mg spectra, at a wavelength longer than 104 nm, our estimated total uncertainty is about 13%. This is accomplished by measuring simultaneously the temperature profile and the total pressure in the heatpipe furnace, which, in turn, are used to derive the column density according to the ideal gas relation. In contrast, the estimated error for spectra in other earlier measurements is typically about 30% due to the uncertainty introduced from the quoted metal vapor density data.

3.2 Results and Discussion

The photoabsorption cross-section $\sigma(\lambda)$ is determined according to the Beer-Lambert law,

$$I(\lambda) = I_o(\lambda)\ exp(-\sigma(\lambda)nL). \tag{1}$$

where $I(\lambda)$ is the transmitted intensity, I_o is the incident intensity, n is the number density, and L is the effective interaction length. In the present experiment, the absolute photoabsorption cross section $\sigma(\lambda)$ is evaluated by replacing nL with $\sum_{i=1}^{25} n_i L_i$ in Eq. (1) to reduce the uncertainty introduced by the use of an estimated effective length. The cross section σ is determined from the slope in the region where $ln(I_o/I)$ varies linearly against nL.

The observed absolute cross sections from the first ionization threshold up to about 105 nm agree very well with the theoretical results from the BSCI calculations by Chang and his co-workers [2, 18, 19], the L^2 calculation by Moccia and Spizzo [4], and the RRPA calculation by Radojevic and Johnson [20]. Fig. 5 compares in detail the measured absolute photoabsorption cross section of Mg in the spectral range from 106 nm to 115 nm with the recent BSCI result by Fang and Chang [19]. The theoretical results are not convoluted and, consequently, the peak cross sections of the narrow $3p\nu d\ ^1P$ resonances are substantially greater than the observed peak cross sections. At lower energy, the experimental result agrees qualitatively with the earlier CI calculation by Bates and Altick and the MCHF (multi-configuration Hartree-Fock approximation) result by Fisher and Saha [4]. Our observed resonance energies also agree well with the values derived from the absorption spectra obtained

by Baig and Connerade [21] and the photoionization spectra by Fiedler *et al* [3]. The present spectra have shown a lot more details than the photoionization experiment by Preses *et al* [3] above the $3p4s$ resonance. It should be noted that the spin-dependent interactions are not included in the BSCI calculation and, as a result, the ^3P resonances that are resolved experimentally on the lower energy side of the $3p\nu s\ ^1P$ resonance are not reproduced theoretically.

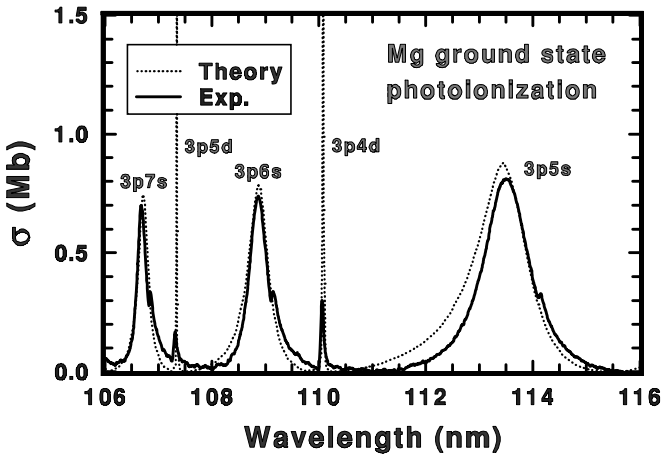

Figure 5. Comparison between measured absolute photoabsorption cross sections and theoretical BSCI results.

Fig. 6 compares the measured photoabsorption cross sections between 75 nm to 90 nm from the ground state of Mg with the theoretical photoionization result from a B-spline-based multichannel K-matrix (BSK) approach by Fang and Chang [10]. The overall agreement in terms of the resonance energy and the spectral profile is again excellent. The only disagreement between theory and experiment is an approximate 0.1 Mb difference in the absolute cross section over the entire spectral region. All three doubly-excited autoionization series, i.e., $4snp$, $3dnp$ and $3dnf\ ^1P$ shown schematically in Fig. 7, are clearly identified from the BSK calculation. The theoretical results are consistent with an earlier L^2-based CI calculation by Mengali and Moccia [22]. It also agrees qualitatively with the result of a close-coupling calculation by Butler *et al.* [23]. The observed resonance energies agree with the data derived from the photoabsorption spectrum of Baig and Conerade [21] up to about 77 nm before they lost the details due to a strongly absorbing continuum in the background.

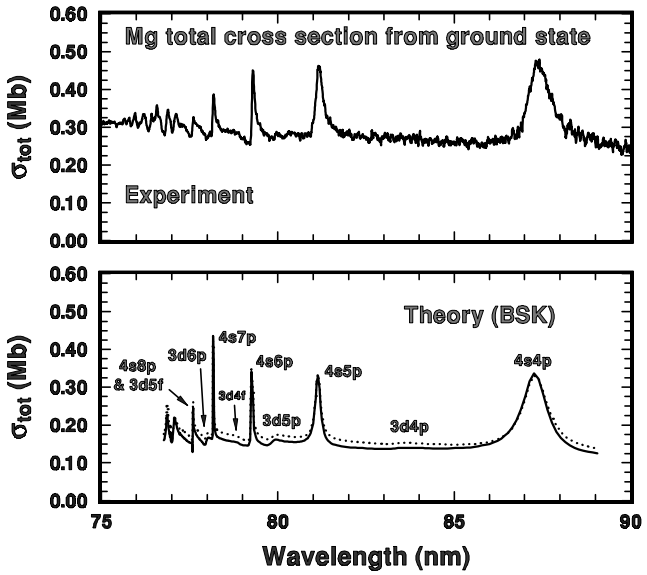

Figure 6. Comparison between measured absolute photoabsorption cross sections and theoretical BSK results between 75 nm and 90 nm.

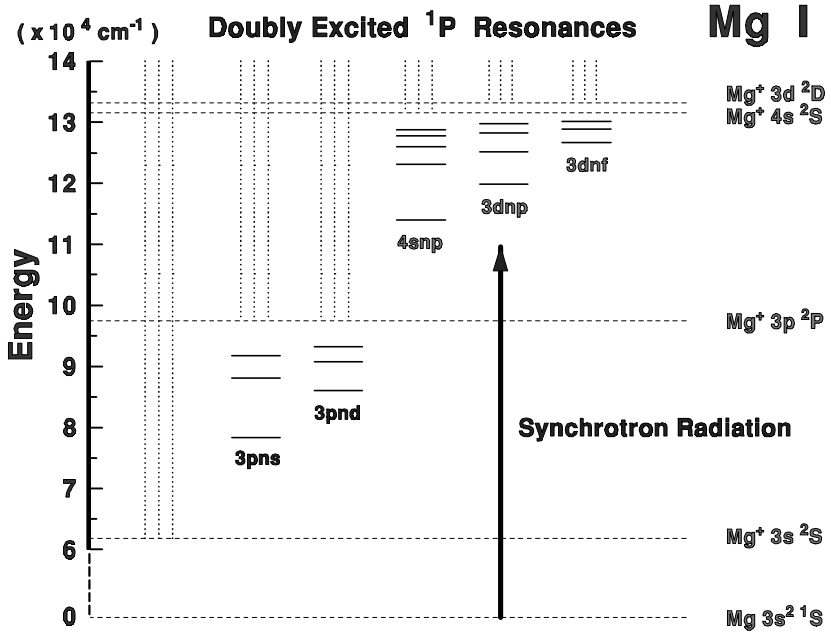

Figure 7. Energy diagram for one photon photoabsorption from the ground state of Mg to the doubly excited ^1P resonances. The vertical dotted lines represent the continua above their respective ionization thresholds.

One of the more interesting features of the spectrum shown in Fig. 6 is the *hidden* $3p4d\ ^1P$ resonance near 83.5 nm. Its presence, though *hidden* both in theoretical and experimental total cross section spectra, is seen clearly in the theoretical partial cross section spectra, at least in two of the ionization channels (i.e., $3p\epsilon s$ and $3p\epsilon d\ ^1P$) shown in Fig. 8. In addition, our calculation shows clearly that the $3p4d\ ^1P$ resonance can be seen unambiguously even in the total ionization spectrum, if the photoionization is originated from the bound excited $3sns\ ^1S$ state [11]. Another interesting feature we have observed in this study is the nearly degenerate overlap between a broad $3d5f$ and a narrow $4s8p$ resonances close to 77.6 nm. In fact, a deatiled analysis based on the theoretical result has shown that the narrow $4s8p$ state is located near the center of the broad $3d5f$ resonance, leading to an appearance of a single resonance. More detailed discussions are presented elsewhere [11].

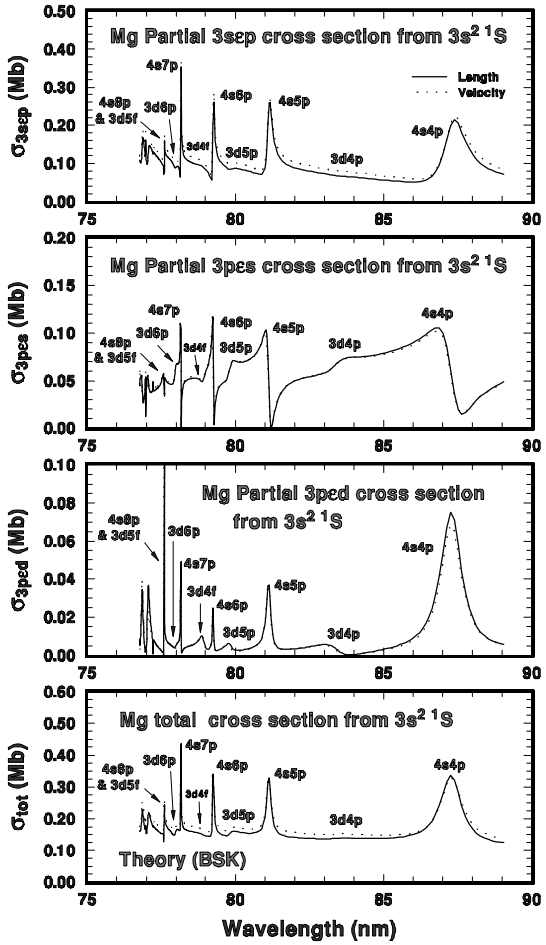

Figure 8. Partial cross sections above Mg $3p$ threshold.

4 Photoionization in the Presence of External Electric Field

In this section, we present the results of a theoretical investigation of the *electric-field effects* on the doubly-excited resonant structures in He ground state photoionization using the complex-rotation method with a BSCI basis [12, 24]. Angular momentum states up to $L_{\max} = 3$ for the final continuum are coupled together by the external electric field. The variations of the structure profiles for the $M_L = 0$ components of He $(2, 2a)$ and $(2, 6a)$ $^1P^o$ and $^1D^e$ resonances for selected dc-electric field strengths are examined. Hopefully, our theoretical findings will stimulate experimental activities in the near future similar to what were reported in Sec. 2 and 3.

4.1 Theory

The complex-rotation method using a BSCI basis employed in this work is presented in detail elsewhere [12]. The photoionization cross section $\sigma\,(E)$ can be parametrized and separated into a non-resonant and a resonant part as [25, 26]

$$\sigma\,(E) = \sigma_0(E) + \sum_{\nu} \sigma_\nu(E) \tag{2}$$

where $\sigma_0(E)$ is the non-resonant background cross section and $\sigma_\nu(E)$ is a modified Fano profile function [27, 28]

$$\sigma_\nu(E) = \sigma_b^\nu \left[\frac{(q_\nu + \varepsilon_\nu)^2}{(1+\varepsilon_\nu^2)} - 1\right] \tag{3}$$

for the ν^{th} resonance at a resonant energy E_ν with a width Γ_ν. The reduced energy ε_ν is given by $\varepsilon_\nu = (E - E_\nu)/\frac{1}{2}\Gamma_\nu$. The profile parameter q_ν is calculated from the ratio of the real and imaginary part of the complex dipole matrix element, B_ν and C_ν, i.e., $q_\nu = -\frac{B_\nu}{C_\nu}$ and $\sigma_b^\nu = 8\pi\alpha\, g(E)\frac{C_\nu^2}{\Gamma_\nu}$, where $g(E) = \Delta E$ and ΔE^{-1} in the length and velocity approximations, respectively. When q_ν, Γ_ν, and σ_b^ν are approximately independent of E over a sufficiently large energy region [27], the resonant strength S_ν of the ν^{th} resonance can be defined as [27, 28]

$$\begin{aligned} S_\nu &= \textstyle\int_{-\infty}^{+\infty} dE\ \sigma_\nu(E) \\ &= \tfrac{\pi}{2}\,\sigma_b^\nu\,\Gamma_\nu\,(q_\nu^2 - 1), \end{aligned} \tag{4}$$

i.e., S_ν represents the area under the modified Fano profile function σ_ν of the ν^{th} resonance.

4.2 Calculations and Results

In the presence of an electric field, M_L remains a good quantum number. For a linearly polarized light with its direction of polarization parallel to the electric

field, the $M_L = 0$ component of a resonant state could be excited from the $^1S^e$ ground state. Angular momentum states with $^1S^e$, $^1P^o$, $^1D^e$, and $^1F^o$ are coupled together to form a BSCI basis of 3680 configurations by the external electric field for the $M_L = 0$ component. We first investigate the He $(2, 6a)$ $^1P^o$ resonant state and a nearby $(2, 6a)$ $^1D^e$ state. For the field-free case, the resonant energy and width for the $(2, 6a)$ $^1P^o$ state are $E_r = -0.514711$ au and $\Gamma = 4.05 \times 10^{-5}$ au, in agreement with the close-coupling results of $E_r = -0.51472$ au and $\Gamma = 3.8 \times 10^{-5}$ au [29]. They are also comparable to $E_r = -0.514732$ au and $\Gamma = 3.67 \times 10^{-5}$ au obtained in a BSCI calculation using an extended BSCI basis with a size over 7000 [26]. As for the $(2, 6a)$ $^1D^e$ state, the field-free resonant energy and width are $E_r = -0.515409$ au and $\Gamma = 6.94 \times 10^{-5}$ au, respectively. Again, they are comparable to the close-coupling results of $E_r = -0.515435$ au and $\Gamma = 6.8 \times 10^{-5}$ au [29].

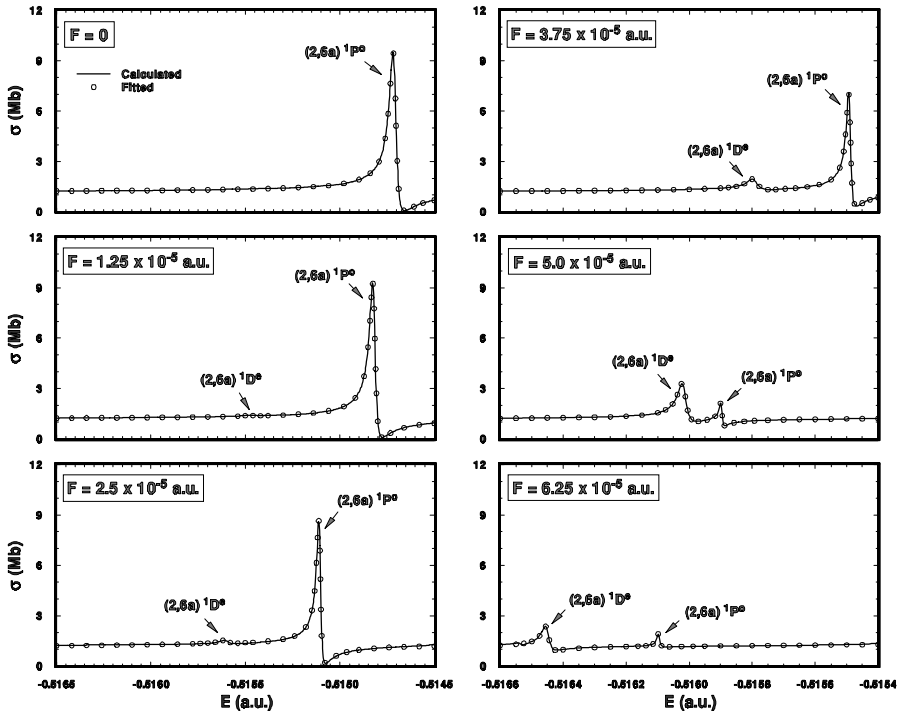

Figure 9. Electric-field effects on He ground state photoionization at varying field strengths F. The solid lines represent the calculated cross sections. The fitted results in open circles are obtained from the parametrized $\sigma(E)$ defined by Eq. (2).

In a rigorous theoretical approach, not only the final state, but also the initial $^1S^e$ ground state should be obtained by including the external electric field to account for the tunnelling effects. However, our calculations have shown that, with the Stark mixing included, the ground state remains a nearly pure $^1S^e$ state for all the electric field strengths under our investigation. A BSCI basis of 3860 configurations,

excluding the tunnelling effect, is used for the strongly correlated He $^1S^e$ ground state in the present calculation. The agreement between the length and velocity results is generally better than 5%. Only velocity results are shown in this report.

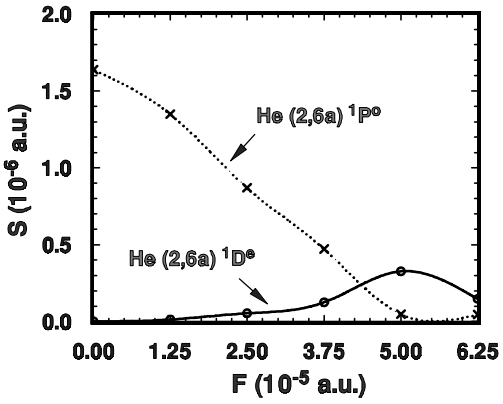

Figure 10. Variation of resonant strengths defined by Eq. (4).

With the presence of external electric field, the calculated cross section $\sigma(E)$ in the energy region around the He $(2,6a)\,^1P^o$ and $(2,6a)\,^1D^e$ resonances is parametrized according to Eq. (2) and the sum over the resonance index ν is limited to the $(2,6a)$ $^1P^o$ and $(2,6a)$ $^1D^e$ states. Note that in the field-free case, the $(2,6a)$ $^1D^e$ state has no contribution to the summation of the parametrized $\sigma(E)$ in Eq. (2). The resonant energy E_ν and width Γ_ν of a state ν are obtained directly from the complex eigenvalue $E_\nu - i\,\Gamma_\nu/2$ and the Fano q-parameter q_ν can be calculated from the ratio between B_ν and C_ν. The weakly energy-dependent background cross sections $\sigma_0(E)$ and σ_b^ν are determined by a linear and a constant fit, respectively. Fig. 9 presents the electric field effects on the resonant structures for the He $(2,6a)\,^1P^o$ and $(2,6a)$ $^1D^e$ states. The solid lines are our calculated photoionization spectra. For a given energy region, about 1000 data points are used to construct the solid curve. The open circles are the parametrized $\sigma(E)$ obtained by using Eq. (2). The agreement between the parametrized $\sigma(E)$ and the calculated one is nearly perfect. For example, at the field strength $F = 5 \times 10^{-5}$ au, the parameters for the parametrized $\sigma(E)$ defined by Eq. (2) are given as $E_r = -0.515896$ au, $\Gamma = 1.02 \times 10^{-5}$ au, $q = -1.98$, and $\sigma_b = 0.284$ Mb for the $(2,6a)\,^1P^o$ state, and $E_r = -0.516017$ au, $\Gamma = 3.21 \times 10^{-5}$ au, $q = -2.87$, and $\sigma_b = 0.251$ Mb for the $(2,6a)\,^1D^e$ state. The background cross section $\sigma_0(E)$ is fitted as $\sigma_0(E) = 37.44 + 70.22E$ Mb, where E is in au. In the absence of electric field, only the $^1P^o$ state can be accessed from the He $^1S^e$ ground state by single-photon absorption. When the external electric field is turned on, the nearby $^1D^e$ resonance is induced by the $^1P^o$ state due to the Stark mixing of these two resonances. The magnitude of the $^1D^e$ resonance first

increases for increasing electric field strength, whereas the magnitude of the $^1P^o$ resonance decreases. Eventually, the $^1P^o$ resonance is practically quenched at about $F = 6.25 \times 10^{-5}$ au ($\sim$ 321 kV/cm). As for the $^1D^e$ state, its magnitude is first increased for increasing field strength until $F = 5 \times 10^{-5}$ au approximately. After that, the quenching effect is also applied to the $^1D^e$ state when the field strength is further increased. The field variations of the resonant strength S of the He $(2, 6a)$ $^1P^o$ and $^1D^e$ states are shown in Fig. 10. Spline fits are used to connect the calculated data points. It can be seen that the $^1D^e$ state attains the maximum resonant strength near $F = 5 \times 10^{-5}$ au.

Similar *quadratic* Stark effect between the $^1P^o$ and $^1D^e$ states is also found in the $(2, 5a)$ pair [12], as well as in the $(2, 3a)$ and $(2, 4a)$ pairs [30]. While the *linear* Stark effect is found in the He $(2, 2a)$ $^1P^o$ and $^1D^e$ pair as shown in Fig. 11, they tend to repel each other for increasing field strength. The magnitude of the $^1P^o$ state is found decreasing when the field strength increases. As for the nearby $^1D^e$ state, its magnitude increases as the field sterength increases. Eventually, its magnitude diminishes as the field strength increases further.

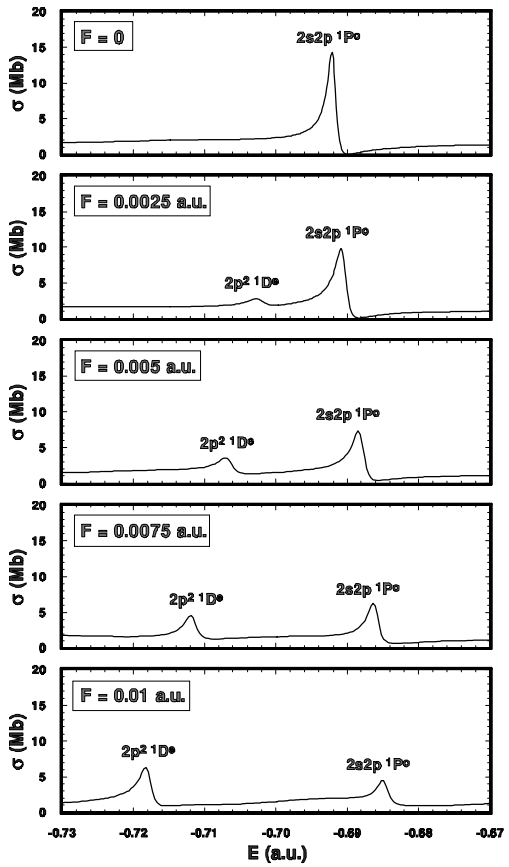

Figure 11. Linear Stark effect due to electric-field effects on He ground state photoionization as the field strengths F varies from 0 to 0.01 au.

5 Concluding Remarks

The joint projects presented in this report, with an extensive interpaly between theory and experiment, have led to remarkable progress to the understanding of the atomic processes dominated by double excitations. The opportunity to work together at the topic program sponsored by the NCTS have benefited all of us tremendously. We have also demonstrated that individual effort contributed by groups from different research institutes, through a stong partnership, may achieve collectively our research object far more efficiently than otherwise.

6 Acknowledgements

We would like to thank NCTS for the sponsorship and, also, K. T. Chung and C. S. Hsu for the organization of the topic program from July through December of 1998. We are grateful for the hospitality extended by T. K. Lee during the topic program at NCTS. This work is supported by Academia Sinica, National Research Council, SRRC, and NSF.

References

[1] T. N. Chang and Y. S. Kim, Phys. Rev. A**36**, 2609 (1986).

[2] T. N. Chang, in *Many-body Theory of Atomic Structure and Photoionization*, ed. by T. N. Chang (World Scientific, Singapore, 1993), p. 213.

[3] J. M. Esteva, G. Mehlman-Balloffet, and J. Romand, J. Quant. Spectrosc. Radiat. Transfer **12**, 1291 (1972); G. Mehlman-Balloffet and J. M. Esteva, Astrophys. J. **157**, 945 (1969); J. P. Preses, C. E. Burkhardt, W. P. Garver, and J. J. Leventhal, Phys. Rev. A**29**, 985 (1984); W. Fiedler, Ch. Kortenkamp, and P. Zimmermann, *ibid.* **36**, 384 (1987).

[4] G. N. Bates and P. L. Altick, J. Phys. B**6**, 653 (1973); C. Froese Fischer and H. P. Saha, Can. J. Phys. **65**, 772 (1987); R. Moccia and P. Spizzo, J. Phys. B**21**, 1145 (1988); R. Moccia and P. Spizzo, Phys. Rev. A**39**, 3855 (1989).

[5] T. S. Yih, H. H. Wu, H. T. Chan, C. C. Chu, and B. J. Pong, Chinese J. Phys. **27**, 136 (1989).

[6] C. C. Chu, H. S. Fung, H. H. Wu and T. S. Yih, J. Phys. B**31**, 3843, (1998).

[7] T. K. Fang, B. I. Nam, Y. S. Kim, and T. N. Chang, Phys. Rev. A**55**, 433 (1997).

[8] A. H. Kung, W. J. Chen, C. K. Ni, T. K. Fang, Y. S. Yih, and T. N. Chang, APS Bulletin, vol. **44**, 722 (1999).

[9] T. N. Chang and X. Tang, Phys. Rev. A**44**, 232 (1991).

[10] T. K. Fang and T. N. Chang, Phys. Rev. A, submitted for publication (1999).

[11] T. S. Yih, H. S. Fung, C. C. Chu, H. H. Wu, T. K. Fang and, T. N. Chang, to be published.

[12] T. K. Fang and Y. K. Ho, Phys. Rev. A**60**, 2151 (1999).

[13] T. K. Fang, Ph. D. thesis, Physics Department, University of Southern California, December 1997 (unpublished).

[14] W. E. Cooke, T. F. Gallagher, S. A. Edelstein, and R. M. Hill, Phys. Rev. Letters **40**, 178 (1978).

[15] T. A. Carlson and M. O. Krause, Phys. Rev. **140**, A1057 (1965); T. A. Carlson, Phys. Rev. **156**, 142 (1967).

[16] S. Bashkin and J. O. Stoner, Jr., *Atomic Energy Levels and Grotian Diagrams I*, (North Holland/American Elsevier, 1975), pp. 388.

[17] Chi-Kung Ni and A. H. Kung, Appl. Opt. **37**, 530 (1998).

[18] T. N. Chang and X. Tang, Phys. Rev. A**46**, R2209 (1992).

[19] T. K. Fang and T. N. Chang, Phys. Rev. A, submitted for publication (1999).

[20] V. Radojevic and W. R. Johnson, Phys. Rev. A**31**, 2991 (1985).

[21] M. A. Baig and J. P. Connerade, Proc. R. Soc, Lond, A**364**, 353, (1978).

[22] S. Mengali and R. Moccia, J. Phys. B**29**, 1597, (1996); 1613, (1996).

[23] K. Butler, C. Mendoza and C. J. Zeippen, J. Phys. B**26**, 4409, (1993).

[24] Y. K. Ho, Phys. Rep. **99**, 1 (1983).

[25] A. Buchleitner, B. Grémaud, and D. Delande, J. Phys. B **27**, 2663 (1994).

[26] T. K. Fang and T. N. Chang, Phys. Rev. A**56**, 1650 (1997).

[27] U. Fano, Phys. Rev. **124**, 1866 (1961).

[28] J. M. Rost, K. Schulz, M. Domke, and G. Kaindl, J. Phys. B **30**, 4663 (1997).

[29] D. H. Oza, Phys. Rev. A **33**, 824 (1986).

[30] T. K. Fang and Y. K. Ho, work in progress.